ACS Catalysis

Research Article

pubs.acs.org/acscatalysis

CO Oxidation at Rutile TiO_2(110): Role of Oxygen Vacancies and Titanium Interstitials

Yan-Yan Yu and Xue-Qing Gong*

Key Laboratory for Advanced Materials, Centre for Computational Chemistry and Research Institute of Industrial Catalysis, East China University of Science and Technology, 130 Meilong Road, Shanghai 200237, People's Republic of China

Supporting Information

ABSTRACT: We present a detailed investigation of the adsorption and oxidation of CO by O_2 at rutile TiO_2(110). PBE, PBE+U, and PBE+U-D methods were tested in calculations to allow a direct comparison of their accuracies. By utilizing the PBE+U-D method, we found that the agreement between theoretical and experimental results has been improved. We then adopted the PBE+U-D method on rutile TiO_2(110) with different defects: i.e., Ti interstitials, O vacancies, or both. It is found that (i) CO adsorbs most favorably at the surface site that undergoes the most significant relaxation upon reduction by such defects, (ii) the O_2 molecule adsorbs as O_2^- or O_2^{2-} at or beside the defects and its dissociation is favorable only when two O^{2-} can occur by accepting the four excess electrons brought by a Ti interstitial, and (iii) the catalytic cycle of CO oxidation by O adatoms from dissociated O_2 can be maintained with the help of Ti interstitials. These results are of importance to understand the role of different defects in metal oxide catalysts.

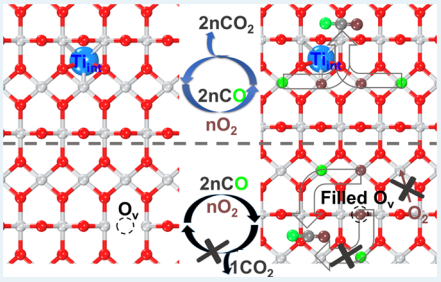

KEYWORDS: *rutile TiO_2, CO adsorption, O_2 activation, CO oxidation, O vacancies, Ti interstitials, density functional theory*

1. INTRODUCTION

Transition-metal oxides have tremendous importance in a wide variety of technological applications such as heterogeneous catalysts, (photo)electrodes, and gas sensors.[1−4] Among them, titanium dioxide (TiO_2) has also become the prototype material for surface science studies largely due to its ordered structure and capability of conduction upon reduction.[2] Rutile TiO_2(110), as the most stable species among various faces of different TiO_2 polymorphs, has attracted much attention for its catalytic activities. In particular, the surface species, including O vacancies, Ti interstitials, and hydroxyl groups,[4−11] are believed to be the active species/sites in various surface processes and they are also of great significance to understand the catalytic properties of other metal oxide surfaces.

CO adsorption and oxidation are prototypical catalytic processes with industrial importance, and they have been widely employed in studying the catalytic performance of TiO_2-based catalysts, though most of these studies were focused on the roles of surface O vacancies,[1,11−15] steps, and interfaces between supported transition-metal clusters and the TiO_2 support.[16−18] Zhao et al.,[19] by combining scanning tunneling microscopy (STM) measurements and density functional theory (DFT) calculations, conducted a comprehensive analysis of CO adsorption at reduced TiO_2(110) containing O vacancies. They successfully located the adsorption sites for CO at the next-nearest-neighbor Ti_{5c} beside the O vacancy, which is different from the native expectation that the O vacancy itself may act as an adsorption site for CO,[15] though the specific reason is unclarified. On the other hand, Ti interstitials' role in catalysis has been rarely explored. In fact, in recent years, there has been growing experimental evidence pointing to the crucial role played by Ti interstitials in surface reduction and subsequent oxidation.[20,21] Besenbacher and Wendt and their co-workers[22] unraveled the diffusion of bulk Ti interstitials in rutile TiO_2(110) by monitoring their reaction with O adatoms. Their STM results showed that the TiO_x islands were formed due to the reaction of outdiffusing Ti^{3+} bulk species with O adatoms. Moreover, they also proposed that Ti interstitials in the near-surface region may be largely responsible for the defect state in the band gap.[23] In addition, CO oxidation as a photocatalytic process has also been carefully investigated in recent studies.[24]

Furthermore, even for the general mechanism of CO oxidation by O_2 adsorbed and activated at surface vacancies, the vacancies are expected to be filled by O from dissociated O_2 after CO_2 formation, leaving a defect-free surface behind which cannot further oxidize CO.[25−27] Therefore, a better catalytic system involving active sites for adsorption and reaction and a sustained catalytic cycle as well are highly desirable. In particular, it has been proposed by Mitsuhara et al. that CO can react with O adatoms properly to form CO_2 at TiO_2,[28,29] implying the importance of O_2 dissociation. Recently, Lira et al.[30,31] revealed in a STM study that a non-vacancy-assisted O_2 dissociation channel may exist, which was also suggested by Wendt et al.[23] to occur within the Ti troughs at TiO_2(110). Most recently, Yoon et al.[32] investigated the potential influence

Received: November 29, 2014
Revised: February 11, 2015
Published: February 17, 2015

DOI: 10.1021/cs501900q
ACS Catal. 2015, 5, 2042−2050

of extrinsic subsurface defects on O_2 dissociation and concluded that Ti interstitials are active when near the surface. However, despite the awareness of the significant role of O_2 adsorption/dissociation at rutile $TiO_2(110)$,[26,33,34] its involvement in CO oxidation have not been well investigated, especially in the case of the existence of Ti interstitials. Hence, a deeper insight into the behavior of Ti interstitials in comparison with O vacancies is still highly demanded and may also help to extend our understanding of catalytic properties of rutile $TiO_2(110)$.

In the current work, we first tested three DFT functionals, i.e. PBE, PBE+U, and PBE+U-D, in order to find a better approach for measuring the interaction between CO and the surface, which was expected to be rather weak.[27] We then proceeded with the study of O_2 adsorption/dissociation and CO oxidation at the rutile $TiO_2(110)$ surface at different active sites, namely Ti interstitials, O vacancies, and both, to provide deeper insights into their roles in the catalytic reactions at defect surfaces. Our results showed that not only the electronic and geometric modifications that take place on the surface due to the occurrence of these active sites can largely affect the reactions but also the intrinsic properties, such as the ability to accept electrons of the adsorbate itself, are important.

2. COMPUTATIONAL DETAILS

All the calculations were carried out using the Vienna ab initio simulation package (VASP).[35,36] Electronic exchange and correlation were treated within the generalized gradient approximation (GGA) by using the Perdew, Burke, and Ernzerhof functional (PBE-GGA).[37] The project-augmented wave (PAW)[38,39] method was used to represent the core−valence electron interaction. The calculations were also conducted involving on-site Coulomb corrections[40,41] (DFT +U, U = 4.2 eV for Ti 3d states as suggested by Deskins et al.[42] and Yoon et al.[32]) and long-range dispersion interactions[43,44] (DFT-D). The titanium 3s, 3p, 3d, and 4s and the carbon and oxygen 2s and 2p electrons were treated as valence electrons. For the comparison of different calculation methods in studying CO adsorption at the surface with O vacancies, the rutile $TiO_2(110)$ slab was modeled using a (4×1) supercell with five trilayers (O−Ti−O), which was reported[25] to be appropriate for the CO reaction, and separated by a ~15 Å vacuum. The valence electronic states were expanded in plane wave basis sets with an energy cutoff of 450 eV, and a Monkhorst−Pack grid of $(1 \times 2 \times 1)$ k points was used. In the calculations of O_2 adsorption/dissociation at the surface with O vacancies and all those concerning the role of Ti interstitials, the surface slab was modeled by a (4×2) supercell, with a 400 eV cutoff energy and a Monkhorst−Pack grid of $(1 \times 1 \times 1)$ k points. In all calculations, the topmost four surface layers as well as the adsorbed molecules were allowed to relax until the atomic forces reached below 0.05 eV/Å.

To estimate the adsorption energies, the following equation was used:

$$E_{ads} = -[E_{M/TiO_2} - E_M - E_{TiO_2}]$$

where E_{M/TiO_2} is the total energy of the interacting systems containing adsorbate M at $TiO_2(110)$ (M = CO, O_2, etc.), and E_M and E_{TiO_2} are energies of the gas-phase molecules and the $TiO_2(110)$ surface slabs, respectively.

The transition states (TS) in reactions were located with a constrained optimization scheme[45] and were verified when (i) all forces on atoms vanish and (ii) the total energy is a maximum along the reaction coordination but a minimum with respect to the rest of the degrees of freedom.

3. RESULTS AND DISCUSSION

A representative structure of rutile $TiO_2(110)$ surface is illustrated in Figure 1. Both fully saturated 3(6)-fold O(Ti)

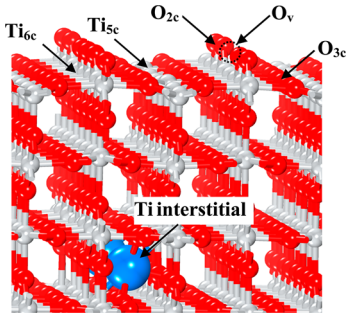

Figure 1. Characteristic ball-and-stick structure of rutile $TiO_2(110)$. The Ti atoms are in gray and O in red. Different surface species are labeled, and Ti interstitials are large balls in blue. These notations are used throughout this paper.

(O_{3c} and Ti_{6c}) and coordinatively unsaturated 2(5)-fold O(Ti) (O_{2c} and Ti_{5c}) are exposed on the surface. It should be noted that, according to the work of Wu et al.,[27] O_2 molecules do not bind to a defect-free surface, and CO oxidation via reaction with lattice oxygen also does not occur on a perfect rutile $TiO_2(110)$ surface. Instead, O_2 binds to a reduced surface and may react with coadsorbed CO. One usual way to reduce the TiO_2 surface is to remove one surface O_{2c}, thereby creating a bridging O vacancy (O_v). Alternatively, the occurrence of Ti interstitials in the bulk can also reduce the surface. It needs to be noted that though both O vacancies and Ti interstitials can reduce the $TiO_2(110)$ surface, their corresponding reduction degrees are quite different: i.e., each O vacancy can give rise to the formation of two Ti^{3+} cations, while one Ti interstitial can bring altogether four Ti^{3+}.

3.1. O Vacancies. The calculated rutile $TiO_2(110)$ surface with one O_{2c} vacancy (O_v) is shown in Figure 2a, together with

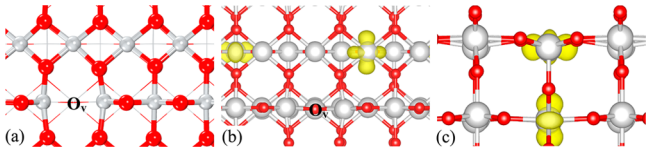

Figure 2. Calculated structure of rutile $TiO_2(110)$ containing one O_{2c} vacancy: (a), (b) top view; (c) side view. The isosurfaces of calculated spin charge (spin-up) densities in (b) and (c) are in yellow, and this notation is used throughout this paper.

the electronic structures (Figures 2b,c). As one can see, introducing one O vacancy gives rise to two excess electrons and they are localized on one 5-fold coordinated Ti at the surface and one 6-fold coordinated subsurface Ti. Previous studies[42,46] hold different views on the exact locations of the localized electrons at reduced $TiO_2(110)$. Chrétien et al.[47] compared the stabilities of all the surface configurations with the localized electrons at different positions, and it was demonstrated that the localization configuration as we determined in this work is relatively the most stable one,

DOI: 10.1021/cs501900q
ACS Catal. 2015, 5, 2042−2050

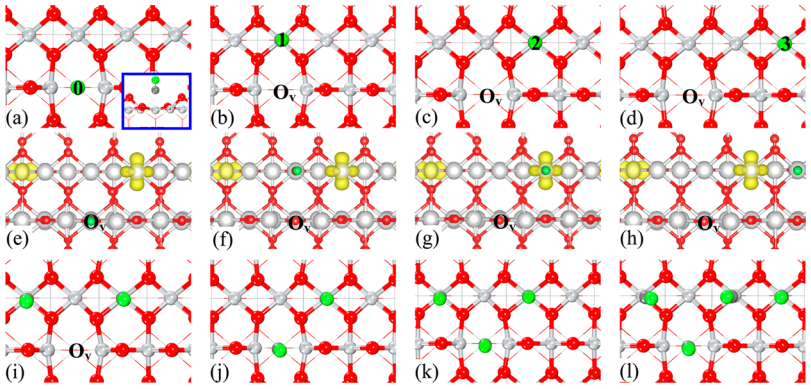

Figure 3. Calculated structures of CO adsorptions at rutile $TiO_2(110)$ with one O_v: (a)−(d) top views of one CO adsorbed at different sites (0−3) (inset of (a) is the side view); (e)−(h) electronic structures of (a)−(d), respectively; (i)−(l): top views of CO coadsorption at 1/2 (i,j), 3/4, and 1 ML coverages.

while the other configurations can be unstable by as much as 0.8 eV. Moreover, studies by using GGA+U and Heyd−Scuseria−Ernzerhof hybrid functional (HSE06) approximations[48,49] have been recently conducted, and it was shown that they give very similar results regarding the energetics and electronic structures of the reduced $TiO_2(110)$ with O vacancies. Therefore, in the current work, this surface configuration was used to characterize the surface processes, including CO adsorption and oxidation.

3.1.1. CO Adsorption. CO adsorption at rutile $TiO_2(110)$ with one O_{2c} vacancy (O_v) was calculated at different surface sites (see Figure 3). According to our calculations, CO is preferentially adsorbed with carbon heading toward exposed Ti in a perpendicular configuration with respect to the surface plane. In addition, the adsorption energies calculated with different methods, i.e. PBE and PBE+U, are also given in Table 1. In the case of the adsorption of a single CO in each 4 × 1 surface cell (coverage 1/4 ML), we tested four different sites: namely O_v itself (0) and the first-nearest (1), second-nearest (2), and the third-nearest (3) Ti_{5c} in addition to O_v. One can see from Table 1 that the adsorption energies obtained with PBE, PBE+U, and PBE+U-D calculations are all quite small. These results clearly indicate that CO adsorption is indeed quite weak at clean $TiO_2(110)$. Moreover, PBE+U and PBE+U-D calculations give consistent results that the second-nearest Ti, which is also one of the reduced Ti cations (Ti^{3+}), is the most favorable site for CO adsorption, followed by the O vacancy, and the third- and first-nearest Ti_{5c}. These results appear to be in line with the STM measurements,[19] in which Wang and Hou and their co-workers observed that CO adsorption follows the Boltzmann distribution and it adsorbs preferentially at such a next-nearest-neighbor Ti_{5c} site close to the O_v.

In order to better understand the relative stabilities of these adsorption states, we further calculated the relaxation of each Ti_{5c} cation upon reduction (O_v formation) by measuring the corresponding root-mean-square (RMS) displacements:[50]

$$r_{\mathrm{RMS}} = \sqrt{\frac{1}{5}\sum_{i=1}^{5}(r_i - r_i^0)^2}$$

where r_i^0 and r_i are the lengths of the five Ti−O bonds of each Ti_{5c} (see Table S1 in the Supporting Information) before and after relaxation, respectively. The calculated r_{RMS} for these Ti_{5c} sites (1−3) are given in Table 2. It can be clearly seen that the larger the r_{RMS}, the greater the adsorption energy of CO, indicating that the adsorption stength is still closely related to the surface relaxation. In other words, the surface Ti cation that undergoes the most significant structural relaxation after the occurrence of O_v is just the Ti^{3+}, and it is also the site where

Table 1. Calculated (Average) Adsorption Energies (in eV) of CO at Rutile $TiO_2(110)$ with One O_v using PBE, PBE+U, and PBE+U-D Methods under Different Coverages

adsorption energy (eV)			
1/4 ML (site)	1/2 ML	3/4 ML	1 ML
PBE Method			
0.30 (0)	0.27	0.25	0.21
0.23 (1)			
0.27 (2)			
0.28 (3)			
PBE+U Method			
0.36 (0)	0.37	0.34	0.30
0.24 (1)			
0.41 (2)			
0.32 (3)			
PBE+U-D Method			
0.52 (0)	0.54	0.50	0.48
0.37 (1)			
0.56 (2)			
0.49 (3)			

Table 2. Calculated r_{RMS} Values (in Å) of Different Surface Ti_{5c} Cations at Defective Rutile $TiO_2(110)$ and Adsorption Energies (E_{ads}, eV) of CO at These Sites

site	E_{ads}	r_{RMS}	Figure
O_v Defect			
1	0.37	0.027	3b
2	0.56	0.126	3c
3	0.49	0.033	3d
Ti Interstitial Defect			
1	0.78/0.72	0.258/0.143	6a/6c
2	0.50/0.47	0.040/0.027	6b/6d
Ti Interstitial + O_v Defect			
1	0.77	0.278	10b
2	0.43	0.038	10c
3	0.44	0.036	10d
4	0.47	0.038	10e

DOI: 10.1021/cs501900q
ACS Catal. 2015, 5, 2042−2050

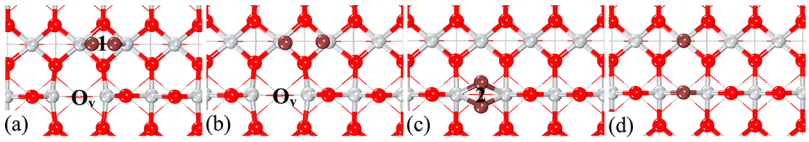

Figure 4. Calculated structures of (a), (c) molecular O_2 and (b), (d) dissociated O_{ad} adsorbed at different sites (1, 2) at rutile TiO_2(110) with one O_v. O_2 and O_{ad} are in brown, and this notation is used throughout this paper.

CO adsorbs most favorably. In addition, it needs to be mentioned that the overall weak adsorption of CO at rutile TiO_2(110) also suggests that PBE+U-D is a better way to describe the related surface processes. In addition, it is also interesting to note that the surface electronic structures, i.e. localizations of the electrons, are not affected at all by the adsorptions (see Figures 3e–h). It then indicates that the adsorptions may not induce significant surface relaxation, which is generally consistent with the calculated rather low adsorption energies.

Under higher coverage (1/2 ML), two COs coadsorbing at two Ti_{5c} sites (for instance, see Figure 3i) and one CO coadsorbing at O_v and the other at Ti_{5c} (see Figure 3j) were considered. By calculating the different adsorption configurations, we found that the former is less stable. Under further increased coverages, such as 3/4 and 1 ML, only the most stable configurations are presented below (see Figures 3k,l).

3.1.2. O_2 Adsorption and Dissociation. The calculated structures for adsorption of O_2 molecule as well as the O atoms (O_{ad}) after O_2 dissociation at rutile TiO_2(110) with one O_v are shown in Figure 4. As has been revealed in previous reports,[23,34,51] O_2 can barely adsorb at stoichiometric rutile TiO_2(110). However, as long as the surface contains defects of O vacancies, O_2 adsorption occurs at both the O_v and nearby Ti_{5c} with relatively high stability. The calculated adsorption energies are given in Table 3. Moreover, we also calculated the dissociation of O_2 at each adsorption site, and the dissociation barriers together with O–O bonds at the transition states are also given in Table 3. For the adsorbed O_2 at Ti_{5c} (site 1, Figure 4a) and O_v (site 2, Figure 4c), the rather long O–O bond lengths (~1.4 Å) clearly indicate that the O_2 groups at both sites are actually doubly charged as O_2^{2-}, which is also evidenced by the varied electronic structures upon its adsorption (see Figure S1 in the Supporting Information). Moreover, from the calculated rather high dissociation barriers (>1 eV) and less stable dissociative states with two O_{ad} at the surface (Figures 4b,d), one may also expect that the adsorbed O_2 molecules cannot undergo dissociation under mild conditions. This can be also understood from the fact that the O_{ad} species are not in their most stable state (O^{2-}) according to our calculations (Figure S1). Nevertheless, we can still determine from Table 3 that paired O_{ad} at Ti_{5c} (Figure 4b) is less stable than the isolated species (Figure 4d), which indicates that O atoms may still tend to fill up the O vacancy.

Table 3. Calculated O_2 Adsorption Energies ($E_{ads}(O_2)$, eV), Dissociation Barriers (E_a, eV), O–O Bonds in the TS (Å), and Adsorption Energies of Coadsorbed O Atoms ($E_{ads}(2O_{ad})$, eV) at Different Adsorption Sites at Rutile TiO_2(110) with Different Defects

site	$E_{ads}(O_2)$	Figure	E_a	O–O	$E_{ads}(2O_{ad})$	Figure
			O_v Defect			
1	1.59	4a	1.78	2.17	−0.22	4b
2	1.97	4c	1.01	2.02	1.32	4d
			Ti Interstitial Defects			
1	2.19	7a	0.38	1.68	3.84	7b
3	2.01	7c			1.50	7d
			Ti Interstitial + O_v Defects			
1	2.11	11a	0	1.67	4.23	11d
2	1.93	11b	0	1.69	5.59	11e
3	1.59	11c	0.57	1.64	2.99	11f

3.1.3. CO Oxidation. For CO oxidation at rutile TiO_2(110) reduced by O vacancies, extensive studies[25−27,52,53] are already available. Consistent with these studies, our results again confirm that the O vacancy is always healed by an O atom left by the O_2 after its reaction with CO. Therefore, the surface with O vacancies may not promote continuous O_2 adsorption and CO oxidation, and these vacancies may not act as sustainable active sites for catalytic processes. It should be noted that previous studies[54,55] showed two O_2 molecules can adsorb as tetraoxygen at one O_v and react with CO. In particular, as Pillay et al.[26] reported, one oxygen atom of the tetraoxygen will react with CO to form CO_2, two O atoms desorb as an O_2 molecule, and finally, the last atom will fill the O vacancy just like the case above. It also needs to be mentioned that, recently, several studies[56−58] have revealed the generation of an oxygen vacancy during the CO oxidation at Au/TiO_2. However, there exist Au clusters and a Au–TiO_2 interface in these systems for CO and O_2 to adsorb and, most importantly, lattice oxygen at the interface may also be activated and react with CO to give rise to CO_2 and a surface O vacancy. This is different from the case of clean TiO_2(110), on which lattice oxygen cannot be activated and CO cannot readily react with it to form CO_2 or the O vacancy either.

3.2. Role of Ti Interstitials. Unlike the case for the bridging O vacancies, Ti interstitials may occur at different locations. The various subsurface interstitials and those between the second and third trilayers have been taken into consideration in our calculations, and the results are presented in Figure 5. From the top view, one may note that the rutile TiO_2(110) surface consists of pentagon-like structural units (see the dashed outlines in blue in Figures 5a,c) involving two Ti_{6c}, two O_{3c}, one Ti_{5c}, and one O_{2c}. Accordingly, the sites right below the center of the pentagon and one side of the pentagon are tested for the occurrence of Ti interstitials. In Figures 5a,c, we present the calculated structures of Ti interstitials at these two sites between the top and second trilayers. According to our calculations, these two interstitials structures have very similar stabilities, with the former being slightly better by 0.03 eV. In addition, for the structures with the Ti interstitials at these two sites between the second and third trilayers (see Figures 5f,h), they have nearly identical stabilities although they are less stable than those of the subsurface Ti interstitials by ~0.4 eV. Moreover, we also tested the sites below the row of the Ti_{5c} (see Figures 5e,j), and the structures with Ti interstitials at such sites between different layers gave much worse stabilities in comparison to those two mentioned above. The corresponding electronic structures of the energetically

DOI: 10.1021/cs501900q
ACS Catal. 2015, 5, 2042–2050

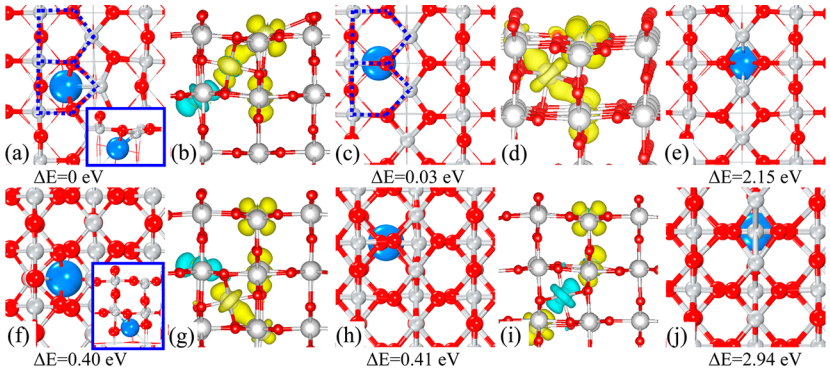

Figure 5. Calculated structures (top view; the insets give a side view) of rutile TiO_2(110) with Ti interstitials;: (a), (c), (e) Ti interstitials between the top and second trilayers; (f), (h), (j) Ti interstitials between the second and third trilayers; (b), (d), (g), (i) corresponding electronic structures of (a), (c), (f), and (h), respectively, with isosurfaces of calculated spin charge densities (spin down in blue). This notation is used throughout this paper.

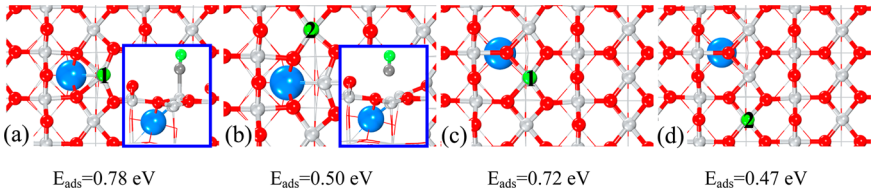

Figure 6. Calculated structures (top view; the insets give a side view) of CO adsorbed at different sites (1, 2) at rutile TiO_2(110) with the Ti interstitials at (a), (b) the sites right below the center of the pentagon and (c), (d) the sites below one side of the pentagon between the top and second trilayers. The corresponding adsorption energies are listed below.

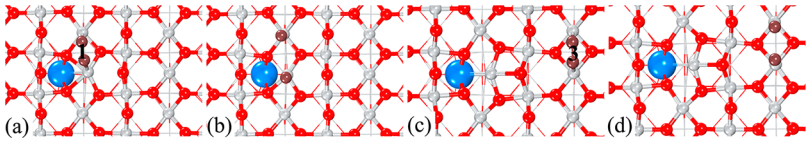

Figure 7. Calculated structures (top view) of molecular O_2 (a), (c) and two O_{ad} (b), (d) after O_2 dissociation at different sites (1, 3) of rutile TiO_2(110) with the most favorable subsurface Ti interstitials.

preferable configurations are presented in Figures 5b,d,g,i, from which one can see the four excess electrons induced by the occurrence of Ti interstitials are localized at different positions of the surface, including the interstitials itself and lattice Ti atoms on the surface and in the bulk.

3.2.1. CO Adsorption. The optimized structures of CO being adsorbed at different sites of rutile TiO_2(110) with energetically preferable subsurface Ti interstitials (Figures 5a,c) are shown in Figure 6, along with the corresponding calculated adsorption energies. The surface Ti_{5c} at the nearest (site 1) and second-nearest (site 2) positions with respect to the Ti interstitials were calculated and compared for CO adsorption. As one can see, for the surfaces with Ti interstitials at the two preferable subsurface sites, CO adsorptions at the nearest Ti_{5c} (Ti^{3+}) are generally more favorable by 0.2−0.3 eV in comparison to those at the second-nearest sites or any other Ti_{5c} farther away (not shown). The corresponding results for Ti interstitials between second and third trilayers are available in Figure S2 and Table S1 in the Supporting Information.

Again, we calculated the r_{RMS} values of the Ti interstitials induced surface relaxation to help in understanding the difference of calculated adsorption energies reported in the above. From the results given in Table 2, one can see that the relaxation of Ti_{5c} at site 1 (0.258/0.143 Å) is indeed much larger than that of site 2 (0.040/0.027 Å). Interestingly, one may also notice that the surfaces with Ti interstitials undergo much more drastic structural relaxation in comparison to those with O vacancies, being largely consistent with the higher CO adsorption energies at the former surfaces.

3.2.2. O_2 Adsorption and Dissociation. At the surface containing a Ti interstitial at the most favorable subsurface site (Figure 5a), we also calculated the adsorption of molecular O_2 and the coadsorption of two O atoms at different surface sites. From the calculated structures presented in Figure 7 and adsorption energies given in Table 3, one may find that O_2 can adsorb at the site just beside the Ti interstitials (site 1) and that far away (site 3) rather strongly, with the adsorption energies being above 2 eV. Moreover, we also found that at the site beside Ti interstitials, the adsorbed O_2 molecule (Figure 7a) can readily dissociate (barrier 0.38 eV) to give rise to the dissociative adsorption state (Figure 7b), which is even more stable by 1.65 eV. On the other hand, the coadsorption of two O atoms at site 3 (Figure 7d) is energetically unfavorable by ~0.5 eV in comparison to the molecular adsorption state. In order to understand these results, we analyzed the changes of the electronic structures upon adsorption and dissociation. As one can see from Figures S3a,b,d in the Supporting Information, the adsorbed molecular O_2 turns out to be O_2^{2-} at the two sites, and at the same time, the number of localized excess electrons generated by Ti interstitials decreases from 4 to 2. Moreover, at site 1 (Figure 7b), each adsorbed O atom from O_2 dissociation appears to be O^{2-} (Figure S3c), while at

DOI: 10.1021/cs501900q
ACS Catal. 2015, 5, 2042−2050

site 3 (Figure 7d), the two adsorbed O atoms share altogether three electrons transferred from the surface, which can be actually identified as an O_2^{3-} species (Figure S3e). Therefore, by comparing the calculated electronic structures of coadsorbed O at the surfaces containing O vacancies and Ti interstitials, we can conclude that four excess electrons are necessary for the favorable dissociation of O_2, which leads to the occurrence of adsorbed O^{2-}; meanwhile, the dissociation site is also important at the surface with Ti interstitials.

Furthermore, O_2 adsorption and dissociation were also investigated at the surface with Ti interstitials in between the second and third trilayers (Figure 5f). The calculation results are given in Table S2 in the Supporting Information. In general, it has been determined that molecular adsorptions at the different sites beside and far away from the interstitials give lower adsorption energies (1.63 and 0.90 eV) in comparison to those at the surface with subsurface Ti interstitials, though O_2 dissociation is still slightly favorable at the nearest Ti sites (1.76 eV). Moreover, it has also been found from the calculated electronic structures (Figure S4 in the Supporting Information) that the O_2 at the surface Ti closest to the interstitials (site 1) turns out to be an O_2^{2-}, and after its dissociation with a barrier of 0.83 eV (see Table S2), two O^{2-} occur. For the case of O_2 at the surface Ti far away from the interstitials (site 3), in contrast, it now turns out to be an O_2^{-}, and it still cannot be completely dissociated: i.e., the O_2^{3-} species occurs (see Figure S4e in the Supporting Information) just like the case of O_2 dissociation at the same site on the surface with subsurface Ti interstitials (Figure S3e in the Supporting Information). By comparing the results of the surfaces containing Ti interstitials in different depths, we can conclude that the excess electrons in deeper bulk Ti atoms are more difficult to transfer to the adsorbate.

3.2.3. CO Oxidation. According to the calculation results of O_2 adsorption and dissociation reported above, a pair of coadsorbed O atoms may readily occur at Ti_{5c} close to the Ti interstitials of TiO_2(110). We then studied the CO oxidation at this site, and the reaction pathway is plotted in Figure 8a. It has been found that CO can first adsorb at another Ti_{5c} beside O_{ad} with the adsorption energy of 0.63 eV. The CO molecule and O_{ad} can combine with each other to react, and at the corresponding transition state, the OC−O_{ad} distance decreases from 2.762 Å in the coadsorption state to 1.688 Å, and the barrier was estimated to be only 0.35 eV. Finally, adsorbed CO_2 occurs at the surface with an adsorption energy of 0.59 eV. After the CO_2 desorbs, the surface is left with a single O_{ad}, which can be involved in the reaction with another CO, as presented in Figure 8b. The overall performance of the latter reaction is quite similar to that of the former, though the calculated adsorption energies for CO (0.74 eV) and CO_2 (0.89 eV) and the barrier (0.45 eV) are all slightly higher. Most importantly, different from the case of the surface with O vacancies, after CO_2 desorbs, this surface recovered as the very beginning one with subsurface Ti interstitials: i.e., a sustainable catalytic cycle for CO oxidation can be properly maintained. Similar schemes at the rutile TiO_2(110) surface with Ti interstitials between the second and third trilayers are available in Figure S5 in the Supporting Information, which gives lower barriers for the reaction (0.03 and 0.20 eV).

3.3. Role of Combined Ti Interstitials and O Vacancies.

Experimental studies have revealed that multiple types of defects, including O vacancies and Ti interstitials, may coexist at TiO_2 nanostructures.[23,30] Therefore, we also calculated the TiO_2(110) surface involving both defects. In particular, the Ti

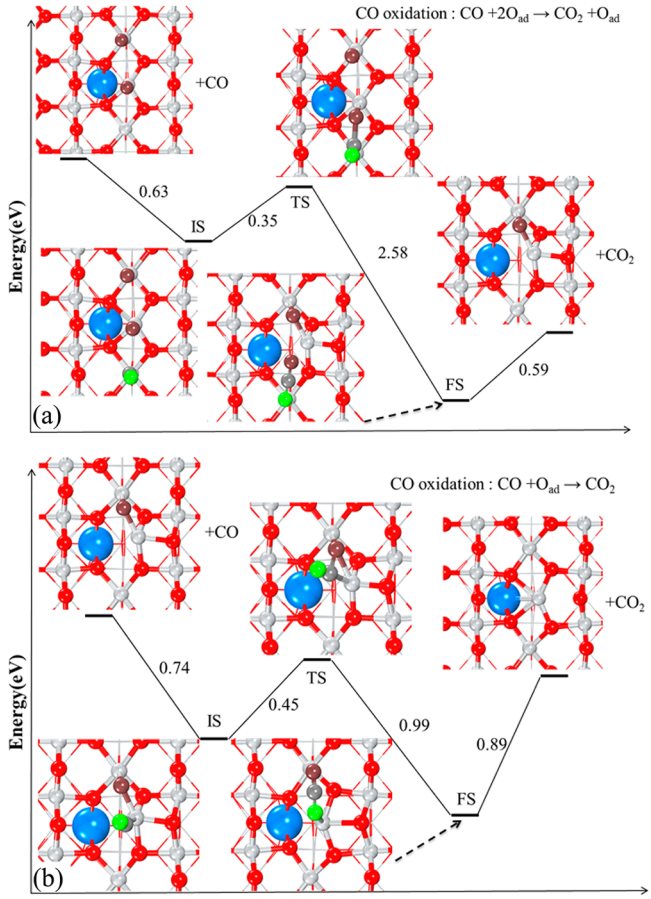

Figure 8. Calculated energy profiles of CO oxidation by (a) paired and (b) single O_{ad} at the rutile TiO_2(110) surface with subsurface Ti interstitials.

interstitial was left at its most favorable subsurface site and the bridge O vacancy was then created at various locations with different distances to the Ti interstitials (see Figure 9). Our calculation results showed that, as the O vacancy moves further away from the interstitials, the surface becomes more stable by up to 1 eV. From the calculated electronic structures, we can see that the Ti interstitials and O vacancy altogether bring six excess electrons to the surface (see Figure S6 in the Supporting Information). Therefore, it can be expected that proper separation of these two defects may well reduce the unfavorable interaction between localized electrons and then increase the surface stability.

3.3.1. CO Adsorption. At the rutile TiO_2(110) surface with the most favorable configuration of combined Ti interstitials and O vacancies (Figure 9d), we also calculated CO adsorption at several different sites (0−4; see Figure 10). We can tell from the calculated adsorption energies that site 1 (Figure 10b) is obviously much more favorable than the other sites for CO adsorption (0.77 eV). The calculated r_{RMS} value (see Table 2) also provided a good interpretation from a structural point of view, as it gives the much larger value of 0.278 Å at site 1 in comparison with those of other sites (~0.04 Å). It needs to be mentioned that, at the rutile TiO_2(110) involving both Ti interstitials and O vacancies, the relative activities of surface Ti_{5c} sites for CO adsorption are very similar to those at the surface with Ti interstitials only (sites 1 and 2). However, they are very different from those of the sites beside the O vacancies alone: i.e., the nearest (sites 2 and 3) and next-nearest (4) sites

DOI: 10.1021/cs501900q
ACS Catal. 2015, 5, 2042−2050

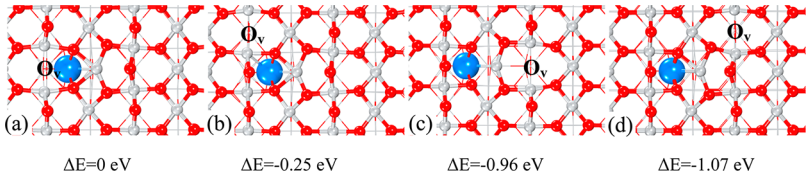

Figure 9. Calculated structures of rutile $TiO_2(110)$ containing both Ti interstitials and O vacancies, with Ti interstitials at the sites right below the center of the pentagon and O vacancies at (a)−(d) four different locations beside the interstitials. The calculated relative total energies are listed below.

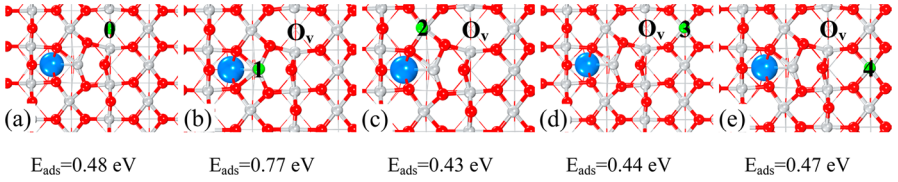

Figure 10. Calculated structures of CO adsorbed at (a)−(e) five different sites (0−4) at rutile $TiO_2(110)$ involving Ti interstitials and O vacancies. The corresponding adsorption energies are listed below.

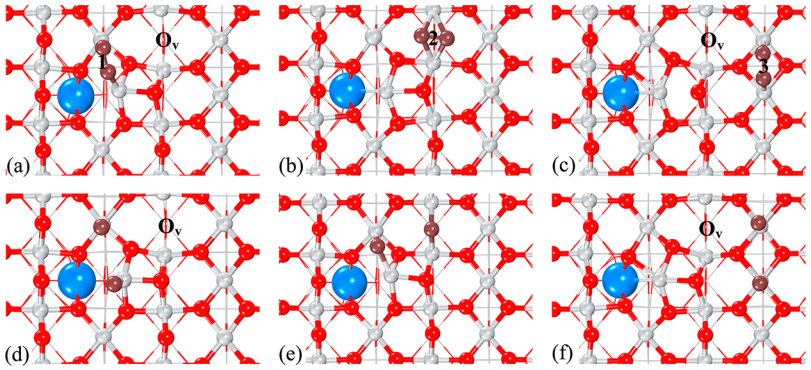

Figure 11. Calculated structures of (a)−(c) molecular O_2 and (d)−(f) pairs of O_{ad} adsorbed at different sites (1−3) of rutile $TiO_2(110)$ with Ti interstitials and O vacancies.

showed almost no difference in CO adsorption while these sites beside O vacancies alone (Figure 3) differed dramatically from each other. Therefore, from the above calculated energetics and structures, we may conclude that, in comparison with O vacancies, Ti interstitials seem to exhibit a more significant role in determining the adsorption strength of CO.

3.3.2. O_2 Adsorption and Dissociation. The calculations of O_2 adsorption and dissociation were also performed at the surface containing both defects. Three different sites (1−3) were considered (see Figure 11). Both molecular and dissociative adsorptions of O_2 were calculated, and from the results given in Table 3, one can see that O_2 readily dissociates at all these sites, with that at site 2 (Figure 11e) being the most favorable to occur. Moreover, in all of these cases, the molecular O_2 and O_{ad} become O_2^{2-} and O^{2-}, respectively, by obtaining two and four excess electrons from the surface (see the electronic structures before and after O_2/O_{ad} adsorption at site 1 in Figure S7 in the Supporting Information). It needs to be mentioned that the O_2 dissociation at site 1 and the O vacancy (site 2) are determined to be barrierless, while there is a barrier of 0.57 eV at site 3, which is rather far away from both Ti interstitials and O_v. This further indicates that not only the number but also the distribution of excess electrons may affect the adsorption and dissociation of O_2. Nevertheless, with Ti interstitials and O vacancies coexisting at the surface, O_2 dissociation is determined to be able to occur much more easily than that at the surface with either Ti interstitials or O vacancies alone.

3.3.3. CO Oxidation. According to the results reported in the above (Table 3), O atoms from dissociated O_2 prefer to fill the O vacancy, leaving behind isolated single O_{ad} on the Ti_{5c} as demonstrated in Figure 11e. Then, CO oxidation would occur exactly in the same way as that plotted in the scheme in Figure 8b.

3.4. Activities of Defective Rutile $TiO_2(110)$. In this work, we have conducted systematic calculations of defective rutile $TiO_2(110)$ surfaces containing O vacancies, Ti interstitials, or both. We also studied the activities of these surfaces by calculating CO adsorption and O_2 adsorption and dissociation, as well as their reactions. From the calculation results, we are able to reveal the activities of the surfaces with different defects regarding their interactions with CO and O_2 as well as promotion effects toward CO oxidation.

For the CO adsorptions, it has been found that they are generally rather weak at the different defective surfaces. However, from the calculated structural properties of the surfaces and the adsorption energies of CO at these surfaces, we still found that the adsorption strength is directly related to the surface relaxation. As one can see from Table 2, no matter which type of defect occurs on rutile $TiO_2(110)$, the surface site that undergoes the most significant relaxation is always the most favorable site for CO adsorption. Considering that the defects of O_v and Ti interstitials also reduce the surface by

DOI: 10.1021/cs501900q
ACS Catal. 2015, 5, 2042−2050

bringing excess electrons and the surface Ti cations undergoing strong relaxation are usually where the excess electrons are localized, we may therefore conclude that both structural and electronic properties of such surface sites can favor CO adsorption.

For the adsorption of O_2, we have found that it generally prefers to sit at the O_v when the vacancy occurs and turns out to be an O_2^{2-} species. However, even though this species is able to directly react with nearby adsorbed CO or dissociate to give rise to O_{ad} at neighboring Ti_{5c} to be involved in reactions, the O_v is always filled up after the reaction/dissociation and cannot give any further promotion effects. In contrast, Ti interstitials are capable of transferring one/two excess electrons to the adsorbed O_2 to turn it into an O_2^-/O_2^{2-} species with rather high adsorption strength and, more interestingly, all four of the excess electrons brought to the surface by each Ti interstitial can even transfer to the pair of adsorbed O_{ad} after O_2 dissociation to turn them into favorable O^{2-} species to promote the dissociation. In addition, after these O^{2-} atoms take part in the CO oxidation, the excess electrons would be left at the surface to promote further O_2 adsorption and dissociation. In other words, sustainable catalytic cycles would be maintained at the surface with such Ti interstitials.

By comparing the calculation results of surfaces with Ti interstitials at different locations, we may further tell that those at the subsurface area are more favorable for involvement in the all-four-electron transfer processes. In contrast, the Ti interstitials at the deeper layers bring excess electrons that are more preferred to be trapped in the bulk area, and their effect to promote O_2 dissociation is less significant. Moreover, O_2 dissociation at different surface Ti_{5c} sites is also sensitive to their distance to the Ti interstitials, and only at the nearest sites can the all-four-electron transfer occur to promote O^{2-} formation.

4. CONCLUSIONS

In summary, by performing systematically DFT calculations with the correction of on-site Coulomb interactions and long-range dispersion interactions, we have studied the adsorption and reaction of CO and O_2 at rutile $TiO_2(110)$ with different types of defects. According to our calculation results, CO adsorbs weakly in general at different sites of rutile $TiO_2(110)$, and its adsorption strength is related to the structural relaxation of the corresponding site upon reduction by surface defects. O_2 adsorption/dissociation can largely change the surface electron structures by accepting the excess electrons from the surface, and the distance between O_2/O_{ad} and excess electrons can also determine the capability of electron transfer. Moreover, in comparison to O_v, the Ti interstitials, each of which can bring four excess electrons to the surface, are more capable of promoting O^{2-} formation as well as O_2 dissociation. More importantly, unlike the O_2 dissociation at O_v which actually fills up the vacancy itself, the O_2 dissociation beside Ti interstitials can provide separate O_{ad} to oxidize CO and at the end of the reactions the surface recovers the original state with the intact Ti interstitials.

■ ASSOCIATED CONTENT

Supporting Information

The following file is available free of charge on the ACS Publications website at DOI: 10.1021/cs501900q.

Calculated lengths of Ti−O bonds and r_{RMS} values of different Ti atoms for CO adsorption, O_2 adsorption, and dissociation, CO oxidation results on the surface containing Ti interstitials between the second and third trilayers, and electronic structures for the surfaces before and after O_2 adsorption/dissociation and the surfaces containing both Ti interstitials and O vacancies (PDF)

■ AUTHOR INFORMATION

Corresponding Author

*X.-Q.G.: e-mail, xgong@ecust.edu.cn; tel, +86 21-64251101.

Notes

The authors declare no competing financial interest.

■ ACKNOWLEDGMENTS

The authors thank the financial support from the National Basic Research Program (2011CB808505), the National Natural Science Foundation of China (21322307, 21421004) and the "Shu Guang" project of Shanghai Municipal Education Commission and Shanghai Education Development Foundation (13SG30). The authors also acknowledge the computing time at the National Super Computing Center in Jinan.

■ REFERENCES

(1) Zhang, W.; Li, Z.; Wang, B.; Yang, J. *Int. J. Quantum Chem.* **2013**, *113*, 89−95.
(2) Sánchez-Sánchez, C.; Garnier, M. G.; Aebi, P.; Blanco-Rey, M.; de Andres, P. L.; Martín Gago, J. A.; López, M. F. *Surf. Sci.* **2013**, *608*, 92−96.
(3) Dohnálek, Z.; Lyubinetsky, I.; Rousseau, R. *Prog. Surf. Sci.* **2010**, *85*, 161−205.
(4) Lun Pang, C.; Lindsay, R.; Thornton, G. *Chem. Soc. Rev.* **2008**, *37*, 2328−2353.
(5) Lira, E.; Wendt, S.; Huo, P.; Hansen, J. Ø.; Streber, R.; Porsgaard, S.; Wei, Y.; Bechstein, R.; Laegsgaard, E.; Besenbacher, F. *J. Am. Chem. Soc.* **2011**, *133*, 6529−6532.
(6) Stausholm-Müller, J.; Kristoffersen, H. H.; Hinnemann, B.; Madsen, G. K.; Hammer, B. *J. Chem. Phys.* **2010**, *133*, 144708−144715.
(7) Papageorgiou, A. C.; Beglitis, N. S.; Pang, C. L.; Teobaldi, G.; Cabailh, G.; Chen, Q.; Fisher, A. J.; Hofer, W. A.; Thornton, G. *Proc. Natl. Acad. Sci. U.S.A.* **2010**, *107*, 2391−2396.
(8) Deskins, N. A.; Rousseau, R.; Dupuis, M. *J. Phys. Chem. C* **2010**, *114*, 5891−5897.
(9) Mulheran, P. A.; Nolan, M.; Browne, C. S.; Basham, M.; Sanville, E.; Bennett, R. A. *Phys. Chem. Chem. Phys.* **2010**, *12*, 9763−9771.
(10) Asaduzzaman, A. M.; Krüger, P. *J. Phys. Chem. C* **2010**, *114*, 19649−19652.
(11) Menetrey, M.; Markovits, A.; Minot, C. *Surf. Sci.* **2003**, *524*, 49−62.
(12) Ji, Y.; Wang, B.; Luo, Y. *J. Phys. Chem. C* **2013**, *117*, 956−961.
(13) Sorescu, D. C.; Yates, J. T. *J. Phys. Chem. B* **2002**, *106*, 6184−6199.
(14) Linsebigler, A.; Lu, G.; Yates, J. T. *J. Chem. Phys.* **1995**, *103*, 9438−9443.
(15) Göpel, W.; Rocker, G.; Feierabend, R. *Phys. Rev. B* **1983**, *28*, 3427−3438.
(16) Green, I. X.; Tang, W. J.; Matthew, N.; Yates, J. T. *Acc. Chem. Res.* **2013**, *47*, 805−815.
(17) Bonanni, S.; Aït-Mansour, K.; Brune, H.; Harbich, W. *ACS Catal.* **2011**, *1*, 385−389.
(18) Singh, J. A.; Overbury, S. H.; Dudney, N. J.; Li, M.; Veith, G. M. *ACS Catal.* **2012**, *2*, 1138−1146.
(19) Zhao, Y.; Wang, Z.; Cui, X. F.; Huang, T.; Wang, B.; Luo, Y.; Yang, J. L.; Hou, J. G. *J. Am. Chem. Soc.* **2009**, *131*, 7958−7959.

DOI: 10.1021/cs501900q
ACS Catal. 2015, 5, 2042−2050

(20) Bowker, M.; Bennett, R. A. *J. Phys.: Condens. Matter* **2009**, *21*, 474224−474232.
(21) Park, K.; Pan, M.; Meunier, V.; Plummer, E. *Phys. Rev. B* **2007**, *75*, 245415−245422.
(22) Zhang, Z.; Lee, J.; Yates, J. T.; Bechstein, R.; Lira, E.; Hansen, J. Ø.; Wendt, S.; Besenbacher, F. *J. Phys. Chem. C* **2010**, *114*, 3059−3062.
(23) Wendt, S.; Sprunger, P. T.; Lira, E.; Madsen, G. K.; Li, Z.; Hansen, J. Ø.; Matthiesen, J.; Blekinge-Rasmussen, A.; Laegsgaard, E.; Hammer, B.; Besenbacher, F. *Science* **2008**, *320*, 1755−1759.
(24) Petrik, N. G.; Kimmel, G. A. *J. Phys. Chem. Lett.* **2013**, *4*, 344−349.
(25) Sorescu, D. C.; Lee, J.; Al-Saidi, W. A.; Jordan, K. D. *J. Chem. Phys.* **2011**, *134*, 104707−104718.
(26) Pillay, D.; Hwang, G. S. *J. Chem. Phys.* **2006**, *125*, 144706−144711.
(27) Wu, X.; Selloni, A.; Nayak, S. K. *J. Chem. Phys.* **2004**, *120*, 4512−4516.
(28) Mitsuhara, K.; Tagami, M.; Matsuda, T.; Visikovskiy, A.; Takizawa, M.; Kido, Y. *J. Chem. Phys.* **2012**, *136*, 124303−124310.
(29) Mitsuhara, K.; Okumura, H.; Visikovskiy, A.; Takizawa, M.; Kido, Y. *Chem. Phys. Lett.* **2011**, *513*, 84−87.
(30) Lira, E.; Huo, P.; Hansen, J. Ø.; Rieboldt, F.; Bechstein, R.; Wei, Y.; Streber, R.; Porsgaard, S.; Li, Z.; Lægsgaard, E.; Wendt, S.; Besenbacher, F. *Catal. Today* **2012**, *182*, 25−38.
(31) Lira, E.; Hansen, J. Ø.; Huo, P.; Bechstein, R.; Galliker, P.; Lægsgaard, E.; Hammer, B.; Wendt, S.; Besenbacher, F. *Surf. Sci.* **2010**, *604*, 1945−1960.
(32) Yoon, Y.; Du, Y.; Garcia, J. C.; Zhu, Z. T.; Petrik, N. G.; Kimmel, G. A.; Dohnalek, Z.; Henderson, M. A.; Rousseau, R.; Deskins, N. A.; Lyubinetsky, I. *ChemPhysChem* **2015**, *16*, 313−321.
(33) Xu, H.; Tong, S. Y. *Surf. Sci.* **2013**, *610*, 33−41.
(34) Pillay, D.; Wang, Y.; Hwang, G. S. *J. Am. Chem. Soc.* **2006**, *128*, 14000−14001.
(35) Kresse, G.; Furthmüller, J. *Comput. Mater. Sci.* **1996**, *6*, 15−50.
(36) Kresse, G.; Furthmüller, J. *Phys. Rev. B* **1996**, *54*, 11169−11186.
(37) Perdew, J. P.; Burke, K.; Ernzerhof, M. *Phys. Rev. Lett.* **1996**, *77*, 3865−3868.
(38) Kresse, G.; Joubert, D. *Phys. Rev. B* **1999**, *56*, 1758−1775.
(39) Blöchl, P. E. *Phys. Rev. B* **1994**, *50*, 17953−17979.
(40) Dudarev, S. L.; Botton, G. A.; Savrasov, S. Y.; Humphreys, C. J.; Sutton, A. P. *Phys. Rev. B* **1998**, *57*, 1505−1509.
(41) Anisimov, V. I.; Aryasetiawan, F.; Lichtenstein, A. I. *J. Phys.: Condens. Matter* **1997**, *9*, 767−808.
(42) Deskins, N. A.; Rousseau, R.; Dupuis, M. *J. Phys. Chem. C* **2011**, *115*, 7562−7572.
(43) Grimme, S. *J. Comput. Chem.* **2006**, *27*, 1787−1799.
(44) Grimme, S. *J. Comput. Chem.* **2004**, *25*, 1463−1473.
(45) Alavi, A.; Hu, P.; Deutsch, T.; Silvestrelli, P. L.; Hutter, J. *Phys. Rev. Lett.* **1998**, *80*, 3650−3653.
(46) Morgan, B. J.; Watson, G. W. *Surf. Sci.* **2007**, *601*, 5034−5041.
(47) Chrétien, S.; Metiu, H. *J. Phys. Chem. C* **2011**, *115*, 4696−4705.
(48) Shibuya, T.; Yasuoka, K.; Mirbt, S.; Sanyal, B. *J. Phys.: Condens. Matter* **2012**, *24*, 435504−435511.
(49) Spreafico, C.; VandeVondele, J. *Phys. Chem. Chem. Phys.* **2014**, *16*, 26144−26152.
(50) Wang, H. F.; Gong, X. Q.; Guo, Y. L.; Guo, Y.; Lu, G. Z.; Hu, P. *J. Phys. Chem. C* **2009**, *113*, 10229−10232.
(51) Wang, Y.; Pillay, D.; Hwang, G. S. *Phys. Rev. B* **2004**, *70*, 193410−193413.
(52) Lee, J.; Zhang, Z.; Deng, X.; Sorescu, D. C.; Matranga, C.; Yates, J. T. *J. Phys. Chem. C* **2011**, *115*, 4163−4167.
(53) Wang, Z.; Zhao, Y.; Cui, X. F.; Tan, S. J.; Zhao, A. D.; Wang, B.; Yang, J. L.; Hou, J. G. *J. Phys. Chem. C* **2010**, *114*, 18222−18227.
(54) Petrik, N. G.; Du, Y.; Dohnalek, Z.; Lyubinetsky; Kimmel, G. A. *J. Phys. Chem. C* **2009**, *113*, 12407−12411.
(55) Kimmel, G. A.; Petrik, N. G. *Phys. Rev. Lett.* **2008**, *100*, 196102−196105.
(56) Widmann, D.; Behm, R. J. *Angew. Chem., Int. Ed.* **2011**, *50*, 10241−10245.
(57) Li, L.; Zeng, X. C. *J. Am. Chem. Soc.* **2014**, *136*, 15857−15860.
(58) Maeda, Y.; Iizuka, Y.; Kohyama, M. *J. Am. Chem. Soc.* **2013**, *135*, 906−909.

DOI: 10.1021/cs501900q
ACS Catal. 2015, 5, 2042−2050